ADVANCED ENERGY MATERIALS
www.advenergymat.de

Boosting the Performance on Scale-Level of Triboelectric Nanogenerators by Controllable Self-Triggering

Qianwang Wang, Xin Yu, Jianlong Wang, Yang Yu, Zhenjie Wang, Zhong Lin Wang, and Tinghai Cheng**

The characteristics of low current and high output impedance of triboelectric nanogenerators (TENGs) constrain their development and application. Recently, corresponding energy management methods have been proposed to solve the problems. Among them, the switch plays an important role in energy management to improve output performance and reduce output impedance. Therefore, a self-triggering switch controlled by TENGs is proposed for power management to achieve high-performance output. It is comprised of an electronic logic switch and the triggering TENG to release the energy stored by the energy-TENG. The experimental results demonstrate that the self-triggering switch can adjust the duty cycle with the assistance of the inherent load characteristics of the TENG. In addition, the coupling output of the two TENGs increases the single-cycle peak current by 137 times (from 32 µA to 4.32 mA) in the vertical contact-separation mode and 5284 times (from 1.3 µA to 6.87 mA) in the horizontal contact mode. In application, the commercial sensor can be powered, and six 100 W lamps in parallel can be lit. The coupling output method of switch-TENGs and energy-TENGs provides important guidance for the development of power management and a new approach toward practical applications.

1. Introduction

As a highly efficient low-frequency energy-harvesting technology,[1] triboelectric nanogenerators (TENGs) have the potential for applications in the energy harvesting of wind,[2] ocean,[3] vibration,[4] human movement,[5] etc.[6] Due to the unique nonlinear resistive and capacitive characteristic, TENGs have the characteristics of low current, and high output impedance.[7]

Research on power management is ongoing and plays an important role in the applications of TENGs. In particular, the switch is applied for the instantaneous release of accumulated energy to increase the output performance. With this solution, the output impedance of the TENG could also be reduced. The TENG with the mechanical switch can achieve an instantaneous release of continuous energy.[8] However, metal contacts are not conducive to integration with the circuit which increases the complexity of the structure.[9] For electronic switches,[10] actuation control is generally achieved by external chemical battery power, which is contrary to the original intention of high-entropy energy harvesting with TENGs. In addition, spark switches have the advantages of a high switching speed and high charge transfer efficiency, however, the impact of the breakdown medium, unstable output performance, and low controllability also limit their application.[11] Therefore, there is an urgent need for a general switch with autonomous controllability, no external chemical power required, high switching speed, and reliability in the TENG field.[12]

In this work, we propose an energy-TENG and switch-TENG coupling strategy for boosting the power output of TENGs. A self-triggering switch controlled by TENG is proposed, which is achieved by the resistive load dividing characteristics of the inherent TENG load characteristics. The experimental results show that the coupling mode single cycle current of the vertical contact separation mode TENG is increased by 137 times (from 32 µA to 4.32 mA). The current of the energy TENG (E_H-TENG) and switch TENG (S_V-TENG) coupled outputs for a single cycle is increased by 5284 times (from 1.3 µA to 6.87 mA). In the application, 120 LEDs in parallel and six 100 W commercial lamps in parallel can be lit. Therefore, the self-triggering switch solved the problem of the adjustability, controllability, and requirement of the external chemical power supply of the TENG. The multiple TENG coupling output method widens the path for the mechanical design of TENGs, and it is easily applied to various energy harvesting design ideas. In addition, it greatly optimizes the development of power management and provides important guidance for the energy management of TENGs.

Q. Wang, X. Yu, J. Wang, Y. Yu, Z. Wang, Z. L. Wang, T. Cheng
Beijing Institute of Nanoenergy and Nanosystems
Chinese Academy of Sciences
Beijing 101400, P. R. China
E-mail: zhong.wang@mse.gatech.edu; chengtinghai@binn.cas.cn
Z. L. Wang
School of Material Science and EngineeringGeorgia Institute of Technology
Atlanta, GA 30332-0245, USA

The ORCID identification number(s) for the author(s) of this article can be found under https://doi.org/10.1002/aenm.202203707.

DOI: 10.1002/aenm.202203707

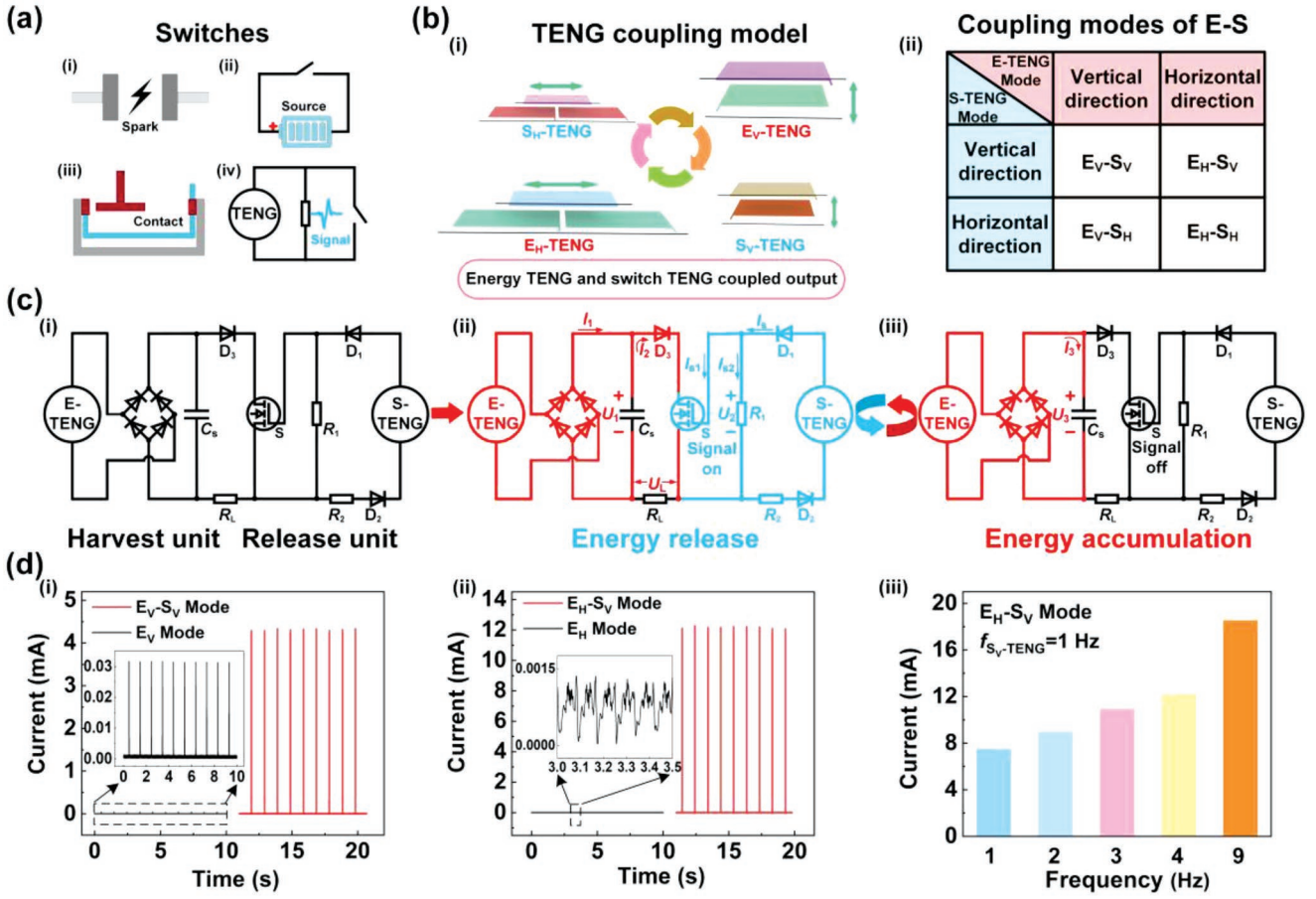

Figure 1. The working mechanism of the self-triggering switch. a) The operating mechanism of conventional switches and the self-triggering switch; i) spark switch, ii) switch with a chemical battery, iii) mechanical contact switch, and iv) the self-triggering switch. b) i) Relationship model and ii) collocation table of the coupled output of the energy-TENG and switch-TENG. c) i) Working principle and process stages of the coupling output circuit. d) i) Output short circuit current of the E_V-S_V mode. ii) Output short circuit current of the E_H-S_V mode. iii) Coupling output current of the E_H-TENG at different frequencies and the S_V-TENG at 1 Hz.

2. Results and Discussion

2.1. Working Mechanism of the Self-Triggering Switch

For a better understanding of the self-triggering switch controlled by TENGs, a comparison of working principles between conventional switches and a self-triggering switch is given. **Figure 1**a shows the spark switch, switch with chemical power source supply, and mechanical contact switch. The working principle of the spark switch is the dielectric breakdown by charge accumulation, and the whole working process is to complete the circuit connection with charge release after the accumulation reaches the dielectric breakdown condition. The switch with an external chemical power supply usually requires a separate chemical battery to control the switch turn-on and turn-off. The principle of the mechanical contact switch is to turn-on and turn-off the circuit in the form of mechanical contact. Figure 1a (iv) shows the theoretical model of the self-triggering switch, which consists of TENG and passive devices. With the electrical signal generated by the TENG model passing through the load resistance, an electrical signal corresponding to the load resistance is generated, which controls the turn-on and turn-off of the logic components. Compared with conventional switches, the self-triggering switch is triggered by a TENG, which has the advantages of high controllability, simple fabrication, high applicability, and no external chemical battery power supply. With the self-triggering switch, a multiple TENG coupling output method is proposed in this paper. In the schematic diagram of Figure 1b (i,ii), the relationship model consists of four basic TENG models: the horizontal direction mode of switch-TENG (S_H-TENG), horizontal direction mode of energy-TENG (E_H-TENG), vertical direction mode of energy-TENG (E_V-TENG) and vertical direction mode of switch-TENG (S_V-TENG).

In Figure 1a (i), the TENG coupling output circuit consists of a harvest unit and a release unit. The connection circuit of the harvest unit is the storage capacitor C_S connected in series at both ends of the rectification bridge. The load resistor, transistor, and diode D_3 are connected in series and connected in parallel at both ends of the storage capacitor C_S, in which the role of diode D_3 is to prevent backflow. The connection circuit of the release unit is an S-TENG, diode D_2, diode D_3, resistor R_1, and resistor R_2 connected in series, in which both ends of the resistor R_1 are connected to the gate and source of the transistor. The role of resistor R_2 could be a current limiting

resistor or voltage divider resistor, which can be used to limit the current when the S-TENG is overcurrent or to share the voltage when the TENG original voltage is too high, and a sliding rheostat can also be used to adjust the signal of resistor R_1 if necessary. Figure 1c (ii) illustrates the working process of the energy release stage. The energy generated by the E-TENG is rectified and stored in the storage capacitor C_S. At the same time, the electrical signal generated by the S-TENG is unidirectionally rectified by diodes D_1 and D_2 to generate a unidirectional electrical signal and then processed by resistor R_1 to generate a unidirectional pulse signal, which can be used to control the turn-on and turn-off of the logic component. According to Kirchhoff's law, the current I_1 and the current I_2 under the electromotive force of the voltage source on the capacitor C_S and original TENG voltage pass through D_3 and the logic transistor which can be regarded as a wire with no resistance as it is turned on, and combined flow through the load resistor R_L. The charge density increased with the two processes of continuous energy storage and instantaneous release working together. Figure 1c (iii) illustrates the working process of the energy accumulation stage, in which the electrical energy generated by the E-TENG is stored on the storage capacitor C_S after being rectified by bridge rectification and the energy cannot be released with the unopened switch.

Figure S2a,b, Supporting Information displays the physical prototypes of the E_V-TENG, S_V-TENG, E_H-TENG, and S_H-TENG. Figure 1d (i) shows that the increased short circuit current of one cycle of the E_V-S_V mode is 4.32 mA, however, the output current of E_V mode is 32 μA. The short circuit current of four cycles of the E_H-S_V mode is increased to 12 mA, however, the output current of E_H mode is 1.3 μA. In Figure 1d (iii), with the working frequency of S_V-TENG in 1 Hz, the trend of linear increase in short circuit current for E_H-TENG of 1, 2, 3, 4, and 9 Hz, verified that the proposed self-triggering switch has adjustable and controllable characteristics.

2.2. Principle of Self-Triggering Switch Circuit

To verify the characteristics of the self-triggering switch circuit, a metal-oxide-semiconductor field-effect transistor (MOSFET) is selected for the experiment, which threshold voltage is 2 V and the turn-on voltage ranges from 2 to 30 V. In this paper, the full mode, contact area, load characteristic and duty cycle of the switch-TENG are investigated comprehensively.

In **Figure 2**a, first, the AC signal generated by the TENG is filtered out the negative half-wave by rectification, leaving only the positive half-wave theoretically. Second, the positive half-wave electrical signal transforms into a pulse signal by flowing through the resistor which depends on the inherent load characteristics of the TENG. In Figure 2b (i) and Figure S2c, Supporting Information, the generated open circuit voltage signals of different areas are verified for the vertical direction mode TENG, in which the areas are 10×10, 15×15, 20×20, 25×25, and 30×30 mm^2. An area of 20×20 mm^2 TENG is selected for testing with load characteristics and duty cycle (Figure 2c (i,ii)). The waveform of the load voltage signal from 3 MΩ to 1000 MΩ verifies that as the load resistance becomes larger, the longer the duration of the electrical signal above 2 V, which makes the duty cycle from 0% to 30%. In Figure 2b (ii) and Figure S2d, Supporting Information, different areas of open-circuit voltage are verified for the TENG in horizontal direction mode, in which the areas are 10×10, 10×15, 10×20, 10×25, and 10×30 mm^2. In Figure 2d (i,ii), an area of 10×30 mm^2 TENG is selected for testing with load characteristics and duty cycle. The waveform of the load voltage signal from 50 MΩ to 10 000 MΩ verifies that as the load resistance becomes larger, the longer the duration of the electrical signal above 2 V, which makes the duty cycle from 0% to 45%. In addition, the verification of the S-TENG is shown in Figure S12 and Video S3, Supporting Information. The characteristics of the switch-TENG are verified by DC power replacing the E-TENG. Figure S12a (i), Supporting Information shows that the LED without a switch could be lit, Figure S13a (ii), Supporting Information shows that the LED could be lit when the transistor has a signal, and Figure S13b (iii), Supporting Information shows that the LED could not be lit when the transistor has no signal.

2.3. Coupling Output Characteristics of E_V-S_V and E_H-S_V Modes

To verify the coupling output method, Figure S2a, Supporting Information displays the prototype set up on one acrylic board to perform the experiments. The voltage signal of the S_V-TENG with $R_1 = 600$ KΩ and $R_2 = 10$ Ω is shown in Figure S3e, Supporting Information. In Figure S1a,b, Supporting Information, the short circuit current of the original signal of the E_V-TENG has a peak value of 32 μA and the open-circuit voltage has a peak value of 300 V.

Figure 3a is a schematic diagram of the coupling of the E_V-TENG and S_V-TENG. Figure 3b shows the output short circuit current of the E_V-TENG and S_V-TENG at different frequencies, which are 0.75, 1.00, 1.25, and 1.50 Hz. The short circuit current increased with increasing frequency, which is related to the increase in the mechanical energy conversion amount by the change in velocity. When the S_V-TENG switch works, the switch is instantly on with a 0.74 μC charge abruptly passing through it (Figure S4a, Supporting Information). Different from other reported switches, this switch can be controlled to turn on at any time and condition by a TENG. In addition, the output short circuit current under different energy storage capacitors C_S is investigated in Figure 3d, and the results show that the maximum output short circuit current is 4.32 mA at 560 nF. The result can be interpreted as follows: when the capacitance is less than 560 nF, the energy storage effect of the capacitor exceeds the filtering effect, when the capacitance is greater than 560 nF, and the filtering effect of the capacitor is greater than the energy storage effect, the filtering and energy storage effects reach an optimal matching value at 560 nF. In Figure S4b, Supporting Information, the short circuit current at 1 Hz shows that the current is very stable, and the switching characteristic is fast and effective. To investigate the current details and charge more clearly, there is a magnified view of 5–6 s in Figure 3c, in which the switch on time is 550 μs and the transferred charge of 0.74 μC matches the V–Q plot, which further validates the accuracy of the experiments.

To better validate the self-triggering switch, the output characteristics with or without switches are tested under the same

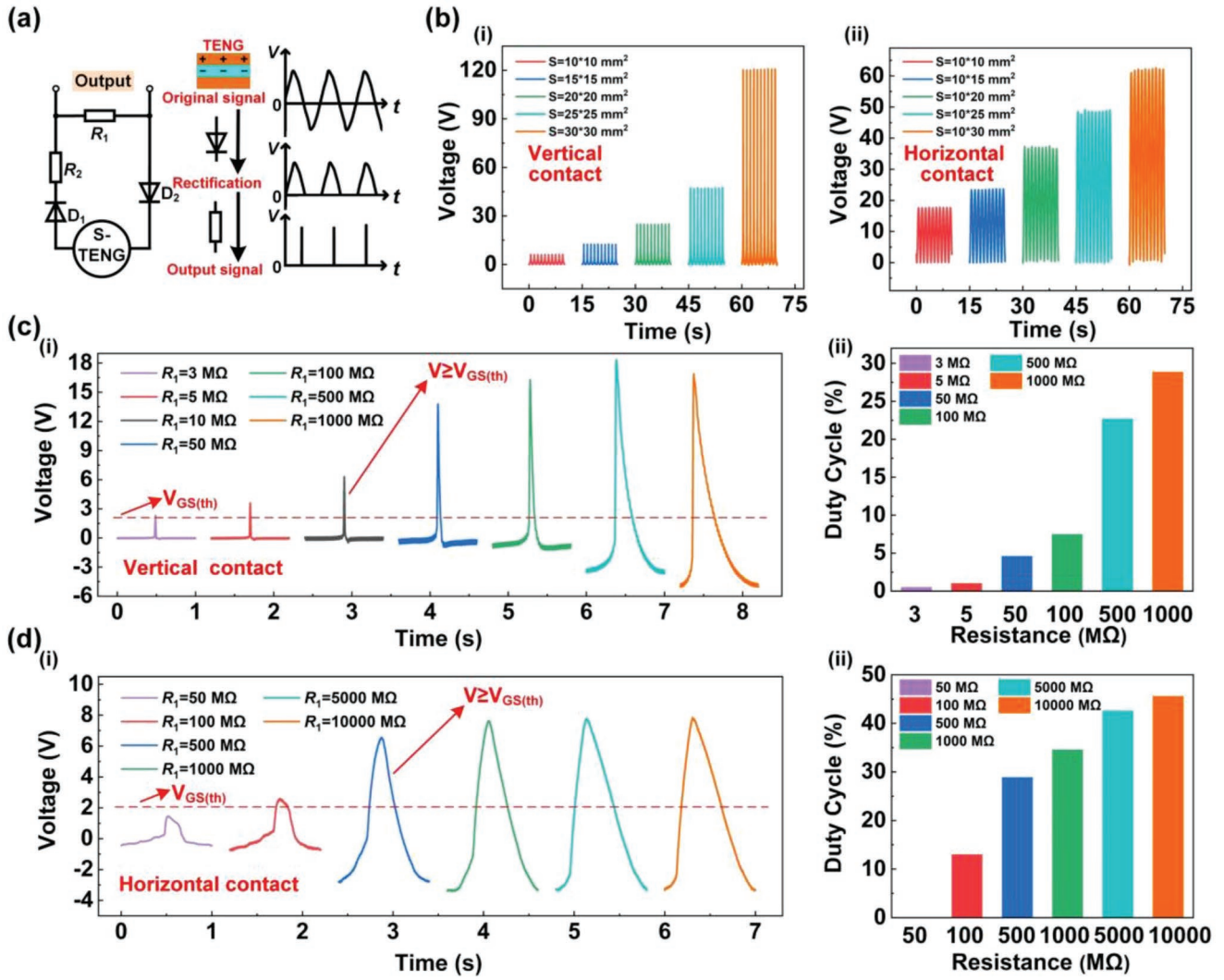

Figure 2. Principle of the self-triggering switch circuit. a) Analysis of the working process. b) i) Output open-circuit voltage of the S_V-TENG at different areas. ii) Open-circuit voltage of the S_H-TENG at different areas. c) i) Output voltage and ii) duty cycle of the S_V-TENG at different resistances. d) i) Output voltage and ii) duty cycle of the S_H-TENG at different resistances.

parameters. In Figures S4c and S6c, Supporting Information, taking 10, 47, and 100 nF capacitors of C_S to do experiments and found that the output voltage performance, when powered by E_V-TENG alone below 100 KΩ, is almost zero and hardly any change, however, the coupled E_V-TENG and S_V-TENG changed greatly at the same condition, which was up to 45 V below 100 KΩ. In Figure 3d and Figure S6d, Supporting Information, at the same load resistance, compared with E_V-TENG working alone, the output current has a large improvement with the coupling E_V-TENG and S_V-TENG. The current reaches milliamp levels at low impedance, however, without energy management, the current is only 32 μA maximum. With the 10 nF storage capacitor, the coupling of the TENG charge transfer characteristics varies with the load as shown in Figure S4d, Supporting Information and Figure 3f. The output short circuit charge diagram of different capacitors is demonstrated in Figure S4e, Supporting Information. The variation curves of the voltage current and peak power with load under different storage capacitors are shown in Figure S7b–d, Supporting Information. The above experimentally measured data verify the feasibility of the switch and the output performance is greatly improved.

Figure 4a shows the schematic diagram of the coupling of E_H-TENG and S_V-TENG. The original output parameters of E_H-TENG is a continuous electrical signal with a peak current value of 1.3 μA and a charge value of 60 nC in Figure S1e–h, Supporting Information.

Figure 4b tests the short circuit current output of S_V-TENG at 1 Hz and E_H-TENG at 0.5, 1.0, 1.5, 2.0, 3.0, and 4.0 Hz, respectively. The verification at different frequencies of E_H-TENG and S_V-TENG is shown in Figure S13, Supporting Information. The output short circuit current increases, as the operating frequency of E_H-TENG increases. In Figure S5a, Supporting Information, when the switch-TENG works, the switch is turned on instantaneously, and the charge 1 μC suddenly passes through. In Figure 4d, different capacitors are tested, and it is found that the short circuit current at 580 nF at 1 Hz

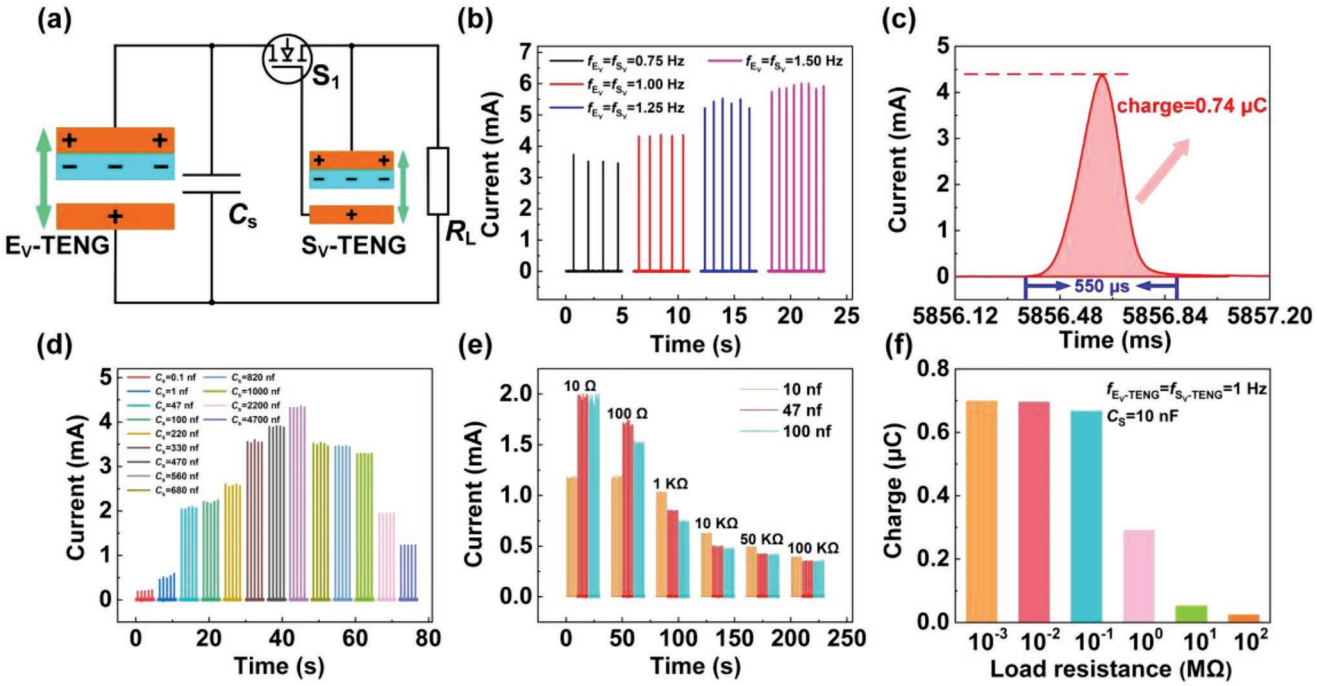

Figure 3. Coupling output characteristics of the E_V-TENG and S_V-TENG. a) Schematic diagram of the E_V-S_V mode. b) Output current at different frequencies. c) Enlarged plot of output current with a 560 nF capacitor at 1 Hz. d) Short circuit current at different capacitances. e) Output current at different capacitances and resistances. f) Transferred charge with a 10 nF capacitor at different resistances.

is 6.8 mA. Figure 4c exhibits the enlarged view of Figure S5b, Supporting Information, it can be seen that the current pulse time is 660 μs, and the charge is 4 μC. To verify the function switch, the output characteristics are tested under the same parameters in Figures S9c and S4c, Supporting Information. In Figure S9d, Supporting Information, the output current is

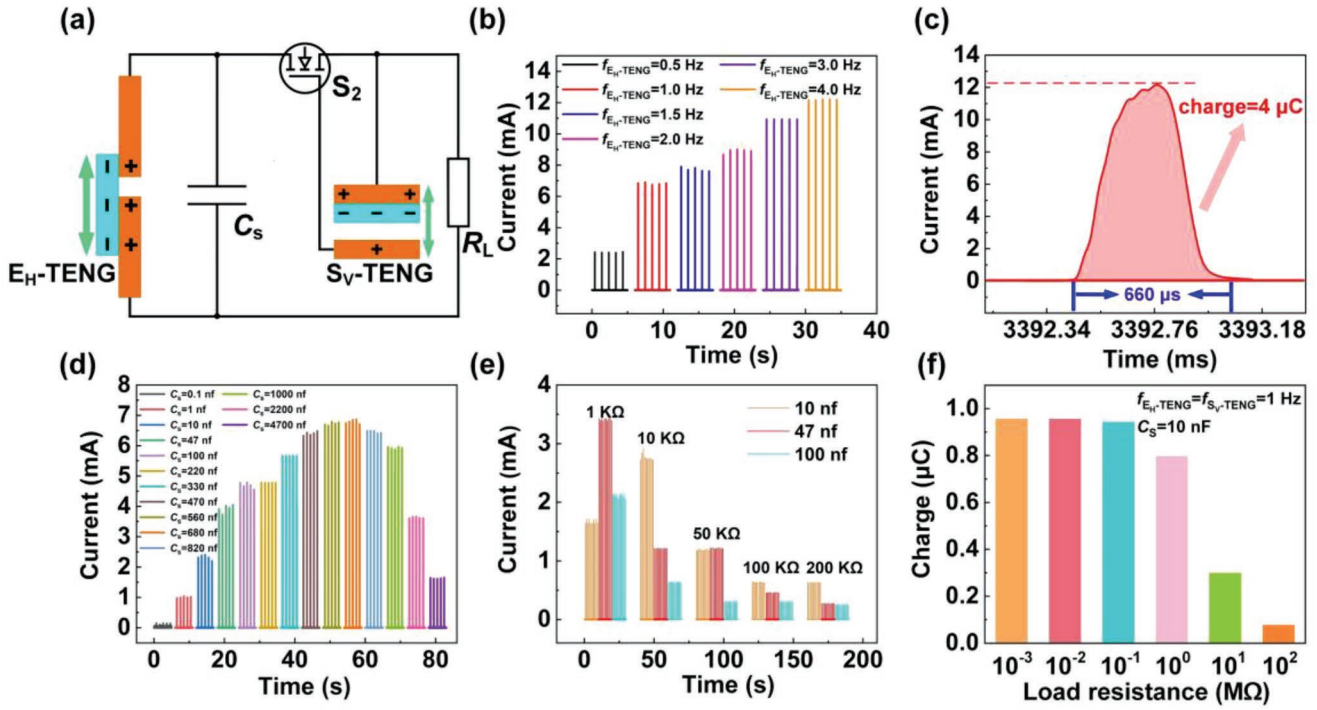

Figure 4. Coupling output characteristics of the E_H-TENG and S_V-TENG. a) Schematic diagram of the E_H-S_V mode. b) Output current of the E_H-TENG at different frequencies and S_V-TENG at 1 Hz. c) Enlarged plot of output current at 4.0 Hz. d) Output current at different capacitances. e) Output current at different capacitances and resistances. f) Transferred charge with a 10 nF capacitor at different resistances.

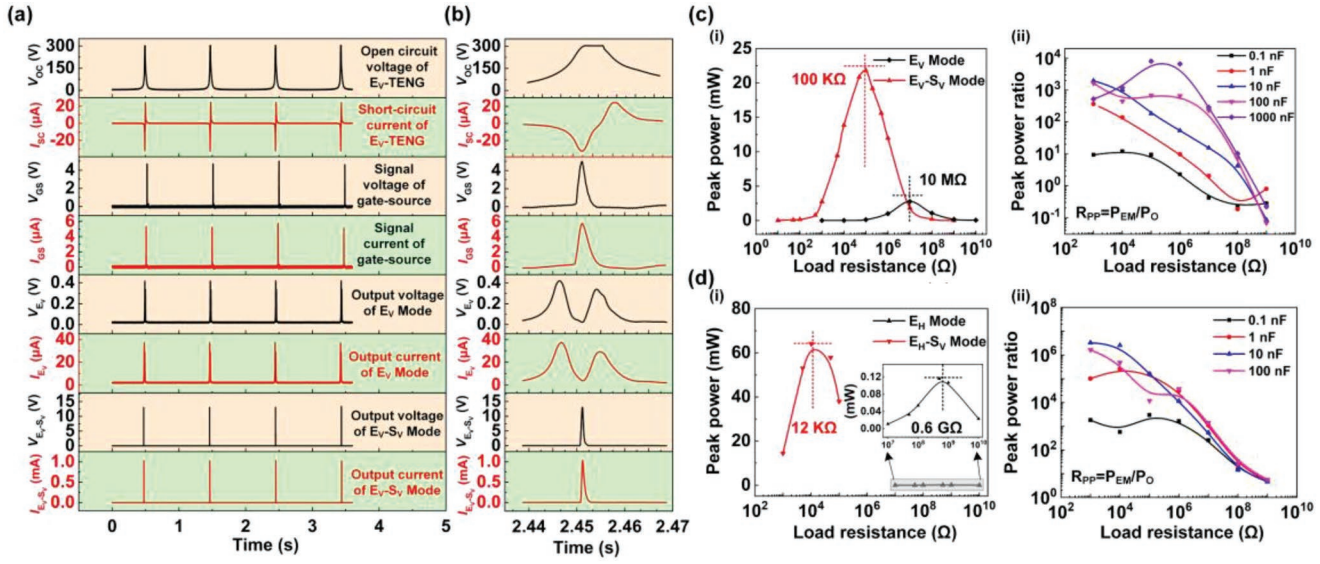

Figure 5. Analysis of performance improvement. a,b) Sequence diagram and its enlarged plot of E_V-S_V mode output (C_S = 10 nF, R_L = 10 KΩ). c) i) Peak power and ii) peak power ratio with different capacitances of E_V-S_V mode. d) i) Peak power and ii) peak power ratio with different capacitances of E_H-S_V mode.

1.6 µA without switching at 1 Hz, and the current decreases with the increasing load resistance. In Figure 4e, the peak current after switching S_V-TENG can reach the milliamp level. Figure 4f and Figure S5d, Supporting Information show the change of the charge transfer characteristics with the load with the storage capacitor is 10 nF. Figure S10, Supporting Information shows the coupling output performance of E_H-TENG and S_V-TENG at 1 Hz. Figure S8, Supporting Information shows the coupling output performance of E_V-TENG and S_H-TENG at 1 Hz. Figure S8a, Supporting Information is the schematic diagram. Figure S8b–d, Supporting Information shows the output characteristic curves of peak voltage and peak current at different capacitances and resistances. Figure S8d, Supporting Information shows the peak power curves at different storage capacitances and resistances, which is greatly improved compared to the maximum output power in Figure S6e, Supporting Information. Figure S11, Supporting Information shows the coupling output performance of E_H-TENG and S_H-TENG at 1 Hz. Figure S11b,c,f, Supporting Information shows the output characteristic curves of peak voltage, peak current, and peak power at different capacitances and resistances. Figure S11d, Supporting Information shows the charge transfer characteristics at different resistances of 10 nF. Figure S11e, Supporting Information shows the short circuit transferred charge at different capacitances. Figure S8, Supporting Information shows the coupling output performance test of E_V-TENG and S_H-TENG. Figure S8b–d, Supporting Information shows the output characteristic curves of peak voltage, peak current, and peak power at different capacitances and resistances.

2.4. Analysis of Performance Improvement

To better explain and illustrate how to achieve the coupling output performance improvement, the following is the sequence diagram of the E_V-S_V mode output with a resistance parameter of 10 KΩ and a capacitance parameter C_S of 10 nF. **Figure 5**a is the sequence diagram. Figure 5b is the enlarged image of the 2–3 s time period in Figure 5a. V_{OC} is the original open-circuit voltage of the E_V-TENG with 300 V, and I_{SC} is the short-circuit current of the E_V-TENG with 32 µA. V_{GS} and I_{GS} are the electrical signals after circuit processing to trigger the transistor. V_{Ev} and I_{Ev} are the output electrical signals of the E_V-TENG after bridge rectification and directly with a resistive load 10 KΩ voltage and current signals, in which the voltage is 0.4 V and the current is 32 µA. $V_{EV\text{-}SV}$ and $I_{EV\text{-}SV}$ are the output voltage and current signals of the coupled E_V-TENG and S_V-TENG, in which the voltage is 13 V, and the current is 1 mA. Compared with the signal without processing, the voltage and current greatly improved. Figure 5 shows a comparison of the peak output power with and without energy management. It can be seen that the output peak power after energy management is 22 mW and the equivalent resistance is 100 KΩ, however, the output power without energy management is 2.2 mW and the equivalent resistance is 10 MΩ, which indicates that the coupling output performance is improved. Figure 5c (ii) demonstrates the peak power ratio (R_{pp}), the ratio of the peak power of E_V-TENG and S_V-TENG coupling outputs to the direct output power of E_V-TENG, which can be explained as:

$$R_{PP} = \frac{P_{EM}}{P_O} \tag{1}$$

The peak power ratio under different capacitances is tested. In Figure 5c (ii), the peak power of the coupling output has a maximum increase of tens of thousands of times at low impedance loads. As the impedance transfer capability of different matched energy storage capacitors is different, a non-linear curve will appear. The comparison with and without energy management is shown in Figure 5. The output peak power with energy management is 62 mW and the equivalent resistance is

12 KΩ, however, the output peak power without energy management is 0.12 mW and the equivalent resistance is 0.6 GΩ. Figure 5d (ii) demonstrates the ratio of the peak power of the coupled output of the E_H-TENG and S_V-TENG to the peak power of the E_H-TENG alone, where the peak power ratios with different capacitances are analyzed, and it can be seen that there is a millions-fold improvement at a low impedance load.

2.5. Demonstration of High-Performance Output

To demonstrate the high output performance of this coupling method, the following applications are used for experimental validation. Series-connected LEDs are suitable for verifying the high voltage characteristic. To verify the high current characteristic, 120 green 5-mm LEDs in parallel and two blue 10-mm LEDs in series are used to test. **Figure 6**a (i),b (i) displays the E_V-TENG separate output schematic diagram and the E_V-TENG and S_V-TENG coupling output schematic diagram. Figure 6a (ii),b (ii) and Video S1, Supporting Information exhibit the LEDs lighting situation, in which can be seen that all LEDs are lit at the coupling output mode. The two series-connected 10 mm LEDs are very bright and the parallel 5 mm LEDs are lit entirely, however, with E_V-TENG working alone, parallel LEDs are not lit and the two series-connected 10 mm LEDs are dark. The lighting time of LEDs in both modes is consistent with the sequence diagram in Figure 5a,b, in which the coupling mode lighting time is short and the working alone mode is long. In Figure 6c (i,ii) and Video S4, Supporting Information, a temperature and humidity sensor can be lit up for work. Figure 6d (i) describes the schematic diagram of the coupled E_V-S_V mode. Figure 6d (ii) exhibits the device of the actual image. Figure 6d (iii) and Video S2, Supporting Information exhibit the successful lighting of six 100 W parallel lamps at 1 Hz. Figure 6e (i)

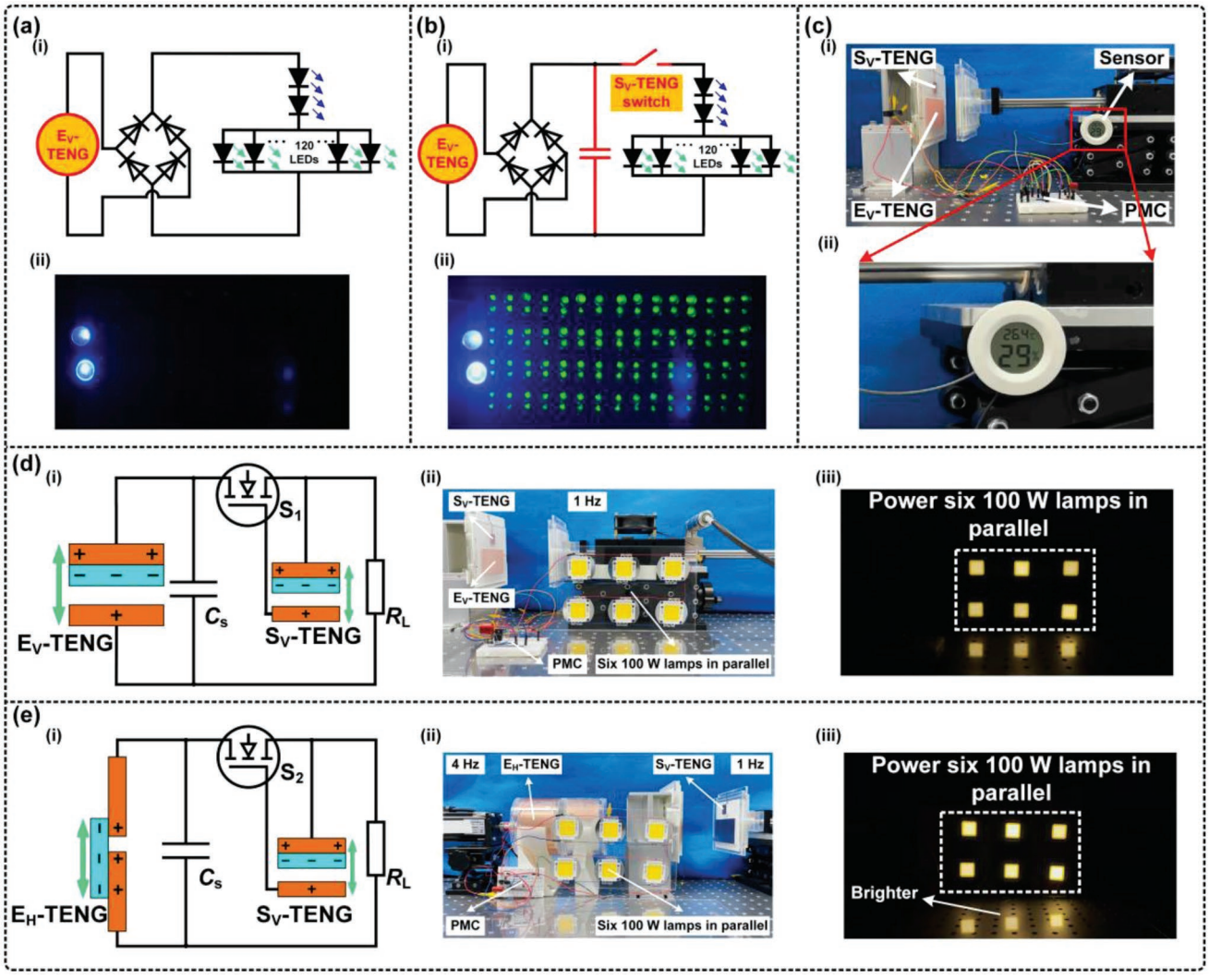

Figure 6. Demonstration of high-performance coupling models. a) Photograph of 120 LEDs in parallel and two blue LEDs in serial powered by TENG without the switch. b) Photograph of 120 LEDs in parallel and two blue LEDs in serial powered by TENG with the switch. c) i,ii) Powering a temperature and humidity sensor. d) Schematic diagram of six 100 W lamps in parallel powered by E_V-S_V mode TENGs. e) Schematic diagram of six 100 W lamps in parallel powered by E_H-S_V mode TENGs.

exhibits the schematic diagram of the E_H-E_V mode. Figure 6e (ii,iii) and Video S2, Supporting Information exhibit the lighting of six 100 W parallel lamps at 4.0 Hz for E_H-TENG and 1 Hz for E_V-TENG, which is brighter than the E_V-S_V mode. To better demonstrate the output performance, demonstrations of the foot pedal and hand press are displayed (Video S5, Supporting Information) and it can be seen that the lighting effect is clearly visible in dark conditions. The above applications verify the function of the self-triggering switch and proved the high performance of coupling model output, and show the great potential for energy management and distributed energy applications. It also provides significant guidance to the next stage of development toward an ultra-high-output power management system.

3. Conclusion

In this paper, a self-triggering switch controlled by TENGs is proposed for power management to achieve a high-performance output, which can effectively convert the continuous dispersed charge distribution into a regular and logically attributed charge distribution. The experimental results show that the coupling mode single cycle current of the vertical contact separation mode TENG increased by 137 times (32 μA to 4.32 mA). The current of the E_H-TENG and S_V-TENG coupled outputs for a single cycle increased by 5284 times (1.3 μA to 6.87 mA). Owing to the extraordinary performance, six 100 W commercial lamps and 120 LEDs in parallel can be lit. The coupling output method by the arrangement of multiple TENGs widens the path for the mechanical design of TENGs, which are easily applied to various energy harvesting fields. In addition, it also demonstrates a framework for high-performance output. Meanwhile, it shows great potential in the field of micro/nano energy harvesting and provides important guidance for the energy management of TENGs.

4. Experimental Section

Fabrication of the Vertical TENG: A laser cutter was used to fabricate various dimensions of a 5 mm thick acrylic plate as a substrate. A sponge adhesive with a thickness of 2 mm was used as a soft contact layer to adhere to the acrylic plate substrate. A copper film with a thickness of 50 μm adhered to the sponge as the dielectric friction layer. A polytetrafluoroethylene (PTFE) film with a thickness of 80 μm adhered to the copper film. Another same copper film as the dielectric friction layer adhered on another identical acrylic board.

Fabrication of the Horizon TENG: In terms of the stator, the size of an acrylic drum was a diameter of 120 mm and a height of 90 mm. Six pairs of copper films of 50 μm thickness adhered to the internal acrylic drum as the dielectric friction layer. For the rotor, a 100 mm diameter and 60 mm height hollow polylactic acid (PLA) was made as rotor support. Six pieces of fluorinated ethylene propylene (FEP) were evenly fixed on the support.

Electrical Measurement: The E_V-TENG and S_V-TENG were driven by a linear motor (Model: LinMot S01-37/120-C) and the E_H-TENG and S_H-TENG were driven by a commercial stepping motor (Model: DVS DE60HB102). The Keithley 6514 programmed electrometer was employed to measure the output performance, such as open-circuit voltage, short-circuit current, and transferred charge. In addition, the measured data were stored and displayed by the data acquisition card (Model: NI-6218B) and the computer, respectively.

Supporting Information

Supporting Information is available from the Wiley Online Library or from the author.

Acknowledgements

Q.W, X.Y., and J.W. contributed equally to this work. The authors are grateful for the support received from the National Key R & D Project from the Minister of Science and Technology (Nos. 2021YFA1201601 & 2021YFA1201604) and the Beijing Natural Science Foundation (No. 3222023).

Conflict of Interest

The authors declare no conflict of interest.

Data Availability Statement

The data that support the findings of this study are available from the corresponding author upon reasonable request.

Keywords

controllable switches, energy management, high performance output, multiple models, triboelectric nanogenerators

Received: November 1, 2022
Revised: December 4, 2022
Published online:

[1] a) F.-R. Fan, Z.-Q. Tian, Z. L. Wang, *Nano Energy* **2012**, *1*, 328; b) Y. Zi, H. Guo, Z. Wen, M.-H. Yeh, C. Hu, Z. L. Wang, *ACS Nano* **2016**, *10*, 4797; c) S. Niu, Z. L. Wang, *Nano Energy* **2014**, *14*, 161; d) Z. L. Wang, *Nano Energy* **2019**, *68*, 104272; e) R. Hinchet, H.-J. Yoon, H. Ryu, M.-K. Kim, E.-K. Choi, D.-S. Kim, S.-W. Kim, *Science* **2019**, *365*, 491.

[2] a) Z. Quan, C. B. Han, T. Jiang, Z. L. Wang, *Adv. Energy Mater.* **2015**, *6*, 1501799; b) Y. Yang, G. Zhu, H. Zhang, J. Chen, X. Zhong, Z.-H. Lin, Y. Su, P. Bai, X. Wen, Z. L. Wang, *ACS Nano* **2013**, *7*, 9461.

[3] a) Z. L. Wang, *Nature* **2017**, *542*, 159; b) G. Liu, H. Guo, S. Xu, C. Hu, Z. L. Wang, *Adv. Energy Mater.* **2019**, *9*, 1900801.

[4] L. Jin, S. Ma, W. Deng, C. Yan, T. Yang, X. Chu, G. Tian, D. Xiong, J. Lu, W. Yang, *Nano Energy* **2018**, *50*, 632.

[5] a) S. Wang, Y. Xie, S. Niu, L. Lin, Z. L. Wang, *Adv. Mater.* **2014**, *26*, 2818; b) Z. L. Wang, *Nano Energy* **2019**, *58*, 669; c) L. Jin, X. Xiao, W. Deng, A. Nashalian, D. He, V. Raveendran, C. Yan, H. Su, X. Chu, T. Yang, W. Li, W. Yang, J. Chen, *Nano Lett.* **2020**, *20*, 6404.

[6] a) X. Pu, H. Guo, J. Chen, X. Wang, Y. Xi, C. Hu, Z. L. Wang, *Sci. Adv.* **2017**, *3*, 1700694; b) J. Chen, Z. L. Wang, *Joule* **2017**, *1*, 480; c) C. Zhang, W. Tang, C. Han, F. Fan, Z. L. Wang, *Adv. Mater.* **2014**, *26*, 3580; d) Z. L. Wang, *Faraday Discuss.* **2014**, *176*, 447; e) Z. L. Wang, *Mater. Today* **2017**, *20*, 74; f) Z. Yang, S. Zhou, J. Zu, D. Inman, *Joule* **2018**, *2*, 642; g) Z. L. Wang, A. C. Wang, *Mater. Today* **2019**, *30*, 34; h) Z. L. Wang, *Rep Prog Phys* **2021**, *84*, 096502; i) C. Wu, A. C. Wang, W. Ding, H. Guo, Z. L. Wang, *Adv. Energy Mater.* **2018**, *9*, 1802906; j) L. Jin, B. Zhang, L. Zhang, W. Yang, *Nano Energy* **2019**, *66*, 104086; k) L. Jin, W. Deng, Y. Su, Z. Xu, H. Meng,

B. Wang, H. Zhang, B. Zhang, L. Zhang, X. Xiao, M. Zhu, W. Yang, *Nano Energy* **2017**, *38*, 185.

[7] a) S. Niu, Y. Liu, Y. S. Zhou, S. Wang, L. Lin, Z. L. Wang, *IEEE Trans. Electron Devices* **2015**, *62*, 641; b) W. Liu, Z. Wang, G. Wang, G. Liu, J. Chen, X. Pu, Y. Xi, X. Wang, H. Guo, C. Hu, Z. L. Wang, *Nat. Commun.* **2019**, *10*, 1426.

[8] a) Y. Zi, J. Wang, S. Wang, S. Li, Z. Wen, H. Guo, Z. L. Wang, *Nat. Commun.* **2016**, *7*, 10987; b) M. A. B. Ouanes, H. Samaali, D. Galayko, P. Basset, F. Najar, *Nano Energy* **2019**, *62*, 465; c) W. Liu, Z. Wang, G. Wang, Q. Zeng, W. He, L. Liu, X. Wang, Y. Xi, H. Guo, C. Hu, Z. L. Wang, *Nat. Commun.* **2020**, *11*, 1883; d) H. Zhang, F. Marty, X. Xia, Y. Zi, T. Bourouina, D. Galayko, P. Basset, *Nat. Commun.* **2020**, *11*, 3221; e) H. Wu, S. Wang, Z. Wang, Y. Zi, *Nat. Commun.* **2021**, *12*, 5470; f) R. Cheng, C. Ning, P. Chen, F. Sheng, C. Wei, Y. Zhang, X. Peng, K. Dong, Z. L. Wang, *Adv. Energy Mater.* **2022**, *12*, 2201532.

[9] a) J. Yang, F. Yang, L. Zhao, W. Shang, H. Qin, S. Wang, X. Jiang, G. Cheng, Z. Du, *Nano Energy* **2018**, *46*, 220; b) H. Zhang, D. Galayko, P. Basset, *J. Phys.: Conf. Ser.* **2019**, *1407*, 012016; c) H. Zhang, D. Galayko, P. Basset, presented at 2019 20th Int. Conf. on Solid-State Sensors, Actuators and Microsystems & Eurosensors XXXIII (TRANSDUCERS & EUROSENSORS XXXIII), Berlin, June **2019**.

[10] a) X. Cheng, L. Miao, Y. Song, Z. Su, H. Chen, X. Chen, J. Zhang, H. Zhang, *Nano Energy* **2017**, *38*, 438; b) F. Xi, Y. Pang, W. Li, T. Jiang, L. Zhang, T. Guo, G. Liu, C. Zhang, Z. L. Wang, *Nano Energy* **2017**, *37*, 168; c) Z. Zhao, J. Liu, Z. Wang, Z. Liu, W. Zhu, H. Xia, T. Yang, F. He, Y. Wu, X. Fu, L.-M. Peng, X. Wei, Y. Hu, *Nano Energy* **2017**, *41*, 351.

[11] a) A. Kawaguchi, H. Uchiyama, M. Matsunaga, Y. Ohno, *Appl. Phys. Express* **2021**, *14*, 057001; b) D. Bao, L. Luo, Z. Zhang, T. Ren, *J. Semicond.* **2017**, *38*, 095001; c) W. Harmon, D. Bamgboje, H. Guo, T. Hu, Z. L. Wang, *Nano Energy* **2020**, *71*, 104642; d) Z. Wang, Q. Tang, C. Shan, Y. Du, W. He, S. Fu, G. Li, A. Liu, W. Liu, C. Hu, *Energy Environ. Sci.* **2021**, *14*, 6627.

[12] a) X. Xia, J. Fu, Y. Zi, *Nat. Commun.* **2019**, *10*, 4428; b) Z. L. Wang, *Adv. Energy Mater.* **2020**, *10*, 2000137.